Physica A 469 (2017) 206–215

Contents lists available at ScienceDirect

Physica A

journal homepage: www.elsevier.com/locate/physa

Singularities of fluctuational paths for an overdamped two-well system driven by white noise

Zhen Chen, Xianbin Liu *

State Key Lab of Mechanics and Control for Mechanical Structures, College of Aerospace Engineering, Nanjing University of Aeronautics and Astronautics, 29 YuDao Street, Nanjing 210016, PR China

HIGHLIGHTS

- Trajectories of different regions of the pattern show distinct properties.
- Topological structure of the Lagrangian manifold and the action surface is considered.
- The quasi-potential of the system is calculated, shown by a contour and 3D plot.
- Bifurcations of singularities are analyzed as the system parameter is changed.

ARTICLE INFO

Article history:
Received 23 August 2016
Received in revised form 3 November 2016
Available online 19 November 2016

Keywords:
Action surface
Lagrangian manifold
Large fluctuations
Quasi-potential

ABSTRACT

Noise-induced escape from a metastable state in an overdamped double-well system is investigated. With the WKB approximation employed, the pattern of fluctuational paths is given. By using the action plot, which gives rise to MPEPs, the pattern is divided into various regions where fluctuational paths inside show qualitatively distinguished characteristics. The global quasi-potential is calculated and its value at the saddle on the boundary agrees with the one obtained by action plot. We show a contour and 3D plot of the quasi-potential to illustrate the relative stabilities of metastable states. The bifurcations of singularities as the system parameter varies are analyzed by the second-order term of the WKB expansion in the vicinity of x axis. Its asymptotic behavior determines the positions of cusps and furthermore, its evolution turns out to delineate the twisting structure of the Lagrangian manifold.

1. Introduction

Dynamical systems are often subjected to weak random perturbations having a profound impact on the dynamics if observations are performed on a sufficient large time scale. For instance, they may result in large fluctuations and noise-induced escape from a locally stable state. Large fluctuations, although occurring only rarely, are responsible for many physical processes, such as protein transport in cells, mutations in DNA sequences and chemical reactions, etc. In the past two decades, a great deal of mathematical and experimental effort has been devoted to the study of large fluctuations in nonequilibrium systems [1–4], using Hamiltonian formalism [5], or equivalent path integral formulations [6,7]. For small random perturbations, the Freidlin–Wentzell theory [8] of large deviations provides a proper framework to depict their effects on dynamics. Put simply, the theory builds on the fact that almost unlikely events, when they occur, do so with an overwhelming probability in the way that is least improbable. The most probable escape path (MPEP) gives rise to the

* Corresponding author.
E-mail addresses: czkillua@icloud.com (Z. Chen), xbliu@nuaa.edu.cn (X. Liu).

http://dx.doi.org/10.1016/j.physa.2016.11.024
0378-4371/

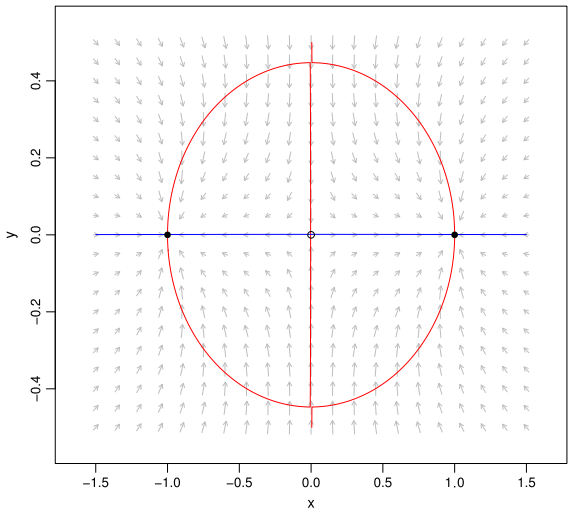

Fig. 1. The deterministic vector field of system (1). The red line is a y-nullcline and the blue line is an x-nullcline. The open circle at the origin is a saddle and filled circles are stable equilibria. We set $\alpha = 5$ and $\mu = 1$. (For interpretation of the references to color in this figure legend, the reader is referred to the web version of this article.)

absolute minimum to some action functional which is the central object of the theory. The quantity of the action serves as the exponential rate of a stationary probability density in the approximated WKB form in the weak noise limit [9]. Its minimum estimates the transition rates between stable states of the original deterministic system and this leads us to another significant quantity introduced in the large deviation theory, that is the quasi-potential.

Singularities such as caustics and cusps [10,11] may arise in the pattern of fluctuational paths due to folding structures of the unstable Lagrangian manifold. This gives rise to a region of the pattern where points are reachable along multiple fluctuational paths. Smelyanskiy, Dykman and Maier [12] topologically investigated the escape from an unstable focus of a periodically oscillating system. They found the Lagrangian manifold has a novel structure with folds spiraling into the focus. D. G. Luchinsky [13] studied a noise driven exit in a double-well system lacking detailed balance and found a bifurcation of MPEP as parameters varied. Their work experimentally demonstrated a series of extraordinary studies by Maier and Stein [14–16] which analytically investigated the asymptotic behavior of the mean first passage time (MFPT) for an irreversible system by the method of WKB approximation and matched asymptotic approximation. Based on that D. G. Luchinsky [17] presented a measurement of an exit location distribution for similar overdamped nonconservative system driven by white noise.

In this paper we investigate the problem in more details. Patterns of fluctuational paths are plotted and divided into various regions within which paths show distinguished behaviors. This is done by an action plot showing multiple local minima. Moreover, the Lagrangian manifold and action surface are given to shed light on the singularities of the pattern. Quasi-potentials of the system is calculated and visualized by a contour and 3D plot. Further studies on the bifurcations of singularities are also performed. This paper is organized as follows. Section 2 introduces the double-well model to be considered in this paper. In Section 3 the WKB approximation is used to give the axillary Hamiltonian system. The pattern and its division are discussed in detail and the associated topological results are given in Section 4. We devote Section 5 to the bifurcations of singularities as the system parameter is changed. Conclusions are drawn in Section 6.

2. Double-well model

The model we investigate is a symmetric double-well one, describing the motion of an overdamped particle in the two-dimensional vector field first proposed in Ref. [14]:

$$\begin{aligned} &\dot{x} = x - x^3 - \alpha x y^2 + \xi_1(t), \\ &\dot{y} = -\mu y - x^2 y + \xi_2(t), \\ &\langle \xi_i(t) \rangle = 0, \qquad \left\langle \xi_i(t)\, \xi_j\left(t'\right) \right\rangle = D\delta_{ij}\left(t - t'\right) \end{aligned} \tag{1}$$

where α and μ are parameters and $\xi_i(t)$ is the white noise of intensity D. For any choice of $\mu > 0$, the deterministic system in the absence of noise has stable points at $(\pm 1, 0)$, a saddle point at $(0, 0)$ and a separatrix along the y axis. The half planes $x > 0$ and $x < 0$ correspond to domains of attraction of stable points $(\pm 1, 0)$ respectively. The vector field is plotted in Fig. 1, together with nullclines and equilibria.

Denoting the vector field by $\mathbf{u}(x, y) = \left(x - x^3 - \alpha x y^2, -\mu y - x^2 y\right)$, it follows that it is not conservative, i.e., a negative gradient of a potential, unless $\alpha = 1$. We set $\mu = 1$ and $\alpha > 0$ throughout this paper. For $\alpha > 0$, we have:

$$\frac{\partial u_x}{\partial y}(x, 0) = 0, \qquad \frac{\partial^2 u_x}{\partial y^2}(x, 0) = -2\alpha x \tag{2}$$

which implies that for any given $x \neq 0$, $u_x(x, y)$ as a function of y attains its local extremum at $y = 0$, i.e., on the x axis. Thus the drifting rate from the saddle toward the stable point decreases as one moves away from the x axis. In other words we can say the attraction of the stable state weakens off the axis. This property has a significant effect on the escape paths and will be clarified later.

3. The WKB approximation

If the noise intensity D is small, the escape from the domain of attraction follows a unique optimal trajectory with overwhelming probability, seemingly in an almost deterministic way. To determine this MPEP, we must turn to investigate the asymptotic solution of the corresponding Fokker–Planck equation as $D \to 0$. In the limit of weak noise intensity D one can seek an approximate solution in an eikonal or WKB form

$$P(\mathbf{x}) \sim C(\mathbf{x}) \exp\left[-S(\mathbf{x})/D\right] \tag{3}$$

with $C(\mathbf{x})$ a prefactor not investigated in this paper and $S(\mathbf{x})$ the activation energy of fluctuations to the vicinity of the point $\mathbf{x} = (x, y)$ in the state space. $S(\mathbf{x})$ is also called quasipotential or nonequilibrium potential [8].

Substituting Eq. (3) into the Fokker–Planck equation and keeping only the terms of lowest order in D, we acquire the Hamilton–Jacobi equation for $S(\mathbf{x})$:

$$H(\mathbf{x}, \mathbf{p}) \equiv \mathbf{u}(\mathbf{x}) \cdot \mathbf{p} + \frac{1}{2}\mathbf{p}^T\mathbf{p} = 0, \quad \mathbf{p} \equiv \frac{\partial S}{\partial \mathbf{x}}. \tag{4}$$

To solve Eq. (4) one can employ the method of characteristics, arriving at the following equations:

$$\frac{\mathrm{d}\mathbf{x}}{\mathrm{d}t} = \frac{\partial H}{\partial \mathbf{p}} = \mathbf{u}(\mathbf{x}) + \mathbf{p} \tag{5}$$

$$\frac{\mathrm{d}\mathbf{p}}{\mathrm{d}t} = -\frac{\partial H}{\partial \mathbf{x}} = -\left[\frac{\partial K(\mathbf{x})}{\partial \mathbf{x}}\right]^T \mathbf{p}. \tag{6}$$

Note that Eqs. (5)–(6) lead to an auxiliary Hamiltonian dynamical system, with the Freidlin–Wentzell Hamiltonian $H(\mathbf{x}, \mathbf{p})$. From this point of view $S(\mathbf{x})$ can be interpreted as the classical action at zero energy [12].

Solutions of Eqs. (5)–(6) describe trajectories yielding extreme values of the cost functional of the form:

$$S[\mathbf{x}(t)] = \int_{t_0}^{t_f} \xi_1^2(t) + \xi_2^2(t)\ \mathrm{d}t \tag{7}$$

with $\mathbf{x}(t)$ being certain trajectory driven by corresponding realization of $\xi_i(t)$ and satisfying $\mathbf{x}(t_0) = \mathbf{x}_0$ and $\mathbf{x}\left(t_f\right) = \mathbf{x}_f$. Using (1) the cost functional (7) can be transformed into an action functional:

$$S[\mathbf{x}(t)] = \int_{t_0}^{t_f} \mathrm{d}t\ L(\mathbf{x}, \dot{\mathbf{x}}), \qquad L(\mathbf{x}, \dot{\mathbf{x}}) = \frac{1}{2}(\dot{\mathbf{x}} - \mathbf{u})^T(\dot{\mathbf{x}} - \mathbf{u}). \tag{8}$$

This has the form of a Lagrangian L for a classical mechanical system. As $D \to 0$, these path integrals (8) can be evaluated by means of steepest descents and the paths dominating the integrals are the ones giving rise to $\delta S/\delta \mathbf{x} = 0$. This results in a Euler–Poisson equation for extreme fluctuational paths which is a $2n$th-order nonlinear partial differential equation. Through applying the following relations [5]:

$$p_i = \sum_{j=1}^{n} (-1)^{j-i} \frac{\mathrm{d}^{j-i}}{\mathrm{d}t^{j-i}} \left(\frac{\partial L}{\partial x^{(j)}}\right) \tag{9}$$

$$H = \sum_i p_i \dot{x}_i - L \tag{10}$$

it can be converted into $2n$ first-order ordinary differential equations, which turn out to be Eqs. (5)–(6). In other words, the action $S(\mathbf{x})$ mentioned above is just defined by the variational problem of (8). Combining (1) and (8)–(10), we have the Freidlin–Wentzell Hamiltonian for (1) as follows

$$H(\mathbf{x}, \mathbf{p}) = \frac{1}{2}\left({p_x}^2 + {p_y}^2\right) + p_x\left(x - x^3 - \alpha x y^2\right) + p_y\left(-y - x^2 y\right) \tag{11}$$

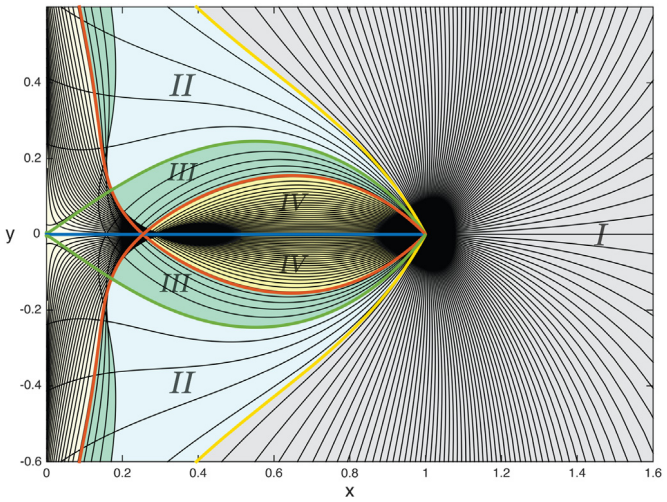

Fig. 2. The pattern of fluctuational paths and various regions in different colors divided by the action plot. The black thin lines are fluctuational paths and the thick lines in colors are boundaries. We set $\alpha = 5$. (For interpretation of the references to color in this figure legend, the reader is referred to the web version of this article.)

and the auxiliary Hamiltonian system

$$\begin{aligned}
\dot{x} &= x - x^3 - \alpha x y^2 + p_x \\
\dot{y} &= -y - x^2 y + p_y \\
\dot{p}_x &= \left(-1 + 3x^2 + \alpha y^2\right) p_x + 2xy p_y \\
\dot{p}_y &= 2\alpha x y p_x + \left(1 + x^2\right) p_y.
\end{aligned} \tag{12}$$

The Hamiltonian flow lies in a four-dimensional phase space spanned by the coordinate $\mathbf{x}$ and the momentum $\mathbf{p}$. It is simple to verify that the original stable points $(\pm 1, 0)$ are hyperbolic saddle points for Hamiltonian system (12) and their unstable manifolds are traced out by fluctuational paths which necessarily satisfy the Euler–Poisson equation as mentioned above. For any point (x, y) in the basin of attraction of $(1, 0)$ for instance, the action $S(x, y)$ is given by integrating the Lagrangian L along the corresponding Hamiltonian trajectory of (12) from $(1, 0)$ to (x, y). It serves as a local minimum of $S[\mathbf{x}(t)]$ over all trajectories $\mathbf{x}(t)$ satisfying $\mathbf{x}(t_0) = (1, 0)'$ and $\mathbf{x}(t_f) = (x, y)'$. Meanwhile the determination of MPEPs requires a minimization over all Hamiltonian trajectories emanating from $(1, 0)$ and reaching outside its basin of attraction.

4. Divisions of the pattern

As pointed out by Ref. [15] the MPEP may bifurcate in the double-well model when the parameter α is changed such that a "focus" or a cusp appears. When $0 < \alpha < 4$, the MPEP is found to locate on the x axis connecting $(1, 0)$ to $(0, 0)$. However, when $\alpha > 4$ singularities appear in the pattern of fluctuational paths which is the main concern of this section.

We show the pattern of fluctuational paths by projecting the Hamiltonian trajectories in four-dimensional phase space into the coordinate space (x, y), plotted by black thin lines in Fig. 2. In the case of $\alpha = 5$, one can see that a cusp point appears on the x axis and there exists a region in which points are reachable by multiple fluctuational paths. The position of this cusp will be determined in Section 6.

Now the method of action plot [3] is employed to give the MPEP in such case. Choosing $(1, 0)$ as the starting point of escape, we can parameterize its unstable manifold, referred to as the Lagrangian manifold, by taking points on a small circle centered at itself. Thus the angular position ϕ is the parameter to trace out the set of trajectories on the Lagrangian manifold. The action plot is then shown in Fig. 3(a), in which 10^5 points on a circle of radius 10^{-6} are used. The Hamiltonian system (12) is integrated until $\mathbf{x}(t)$ enters into the left-half plane, i.e., escapes from the original basin of attraction. An upper bound of time for the integral which is sufficiently large is given since some trajectories do not make such transitions.

Three local minima of the actions are found and clarified in Fig. 3(b). Two of them having global minima of 0.4831 correspond to the green thick lines connecting $(1, 0)$ to $(0, 0)$ in Fig. 2, and the others having local minimum of 0.5 corresponds to the blue line segment on the x axis. This implies that the escape does occur through the saddle point $(0, 0)$ of the vector field $\mathbf{u}(x, y)$ and the MPEP has bifurcated into two off-axis ones. It follows from that as α increases, the off-axis weakness of the attraction of $(1, 0)$ is aggravated, making it easier to fluctuate toward the separatrix off the x axis.

In addition, several typical paths are also plotted in Fig. 2, dividing the pattern into various regions. Trajectories in Region-I do not escape but fluctuate to any terminating point inside, with each path being the optimal one to the current point. The

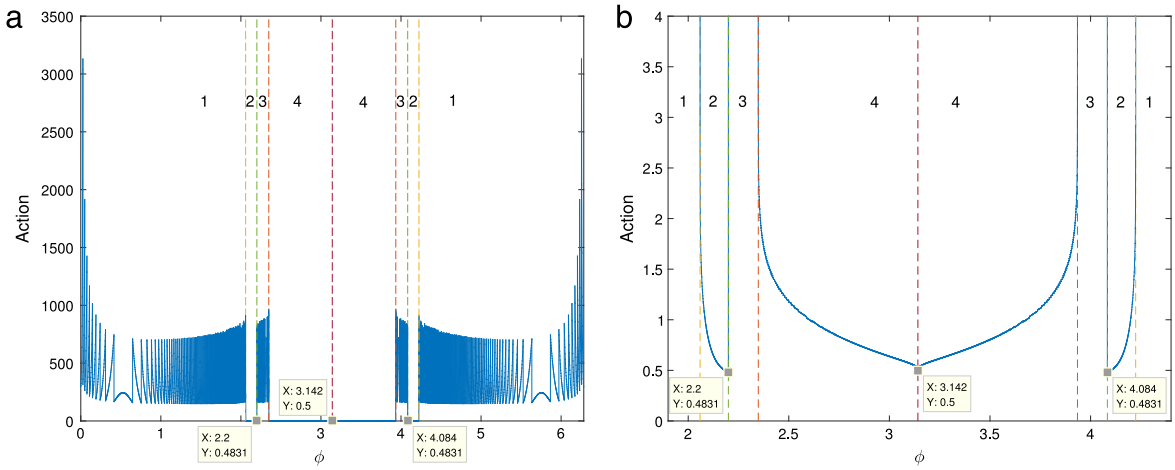

Fig. 3. (a) The action plot for system (12). The x axis is the angular position to parameterize the escape trajectories, ranging from $[0, 2\pi)$. 10^5 points are taken in this range. (b) A local amplification of (a) where the minima are attained. (For interpretation of the references to color in this figure legend, the reader is referred to the web version of this article.)

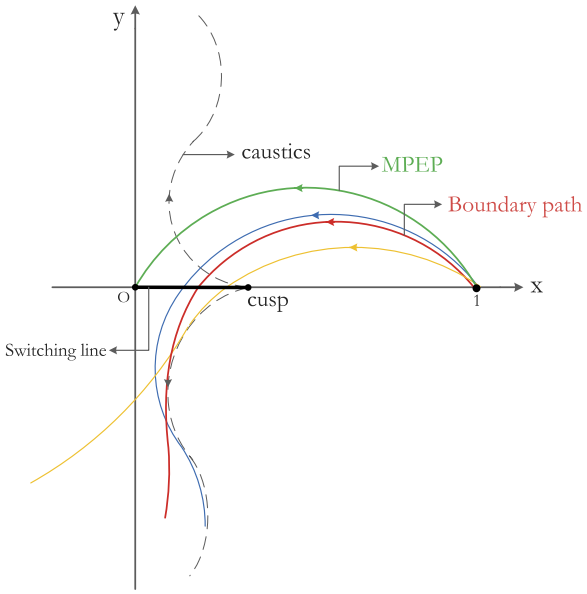

Fig. 4. A schematic illustration of the pattern of fluctuational paths. The caustics are shown in dashed lines, emanating from a cusp point on the x axis. Trajectories in Region-III and IV are plotted in blue and yellow respectively. (For interpretation of the references to color in this figure legend, the reader is referred to the web version of this article.)

two yellow lines in Fig. 2, which serve as boundaries of Region-I, are the asymptotic lines which approach the y axis. It is observed that the values of actions are extremely large since their trajectories do not escape within the given time range. In reality such large actions should not be expected within reasonable length of time since the noise intensity is small. However, the trajectories in Region-I do play certain roles physically in the escaping process, serving as unsuccessful escape attempts. A sample path leaving the diffusion-dominated region of size $O\left(D^{1/2}\right)$ surrounding $(1, 0)$ will follow one of the fluctuational paths in Region-I with high probability and then, relax to the stable point again following a deterministic trajectory satisfying $\dot{\mathbf{x}} = \mathbf{u}(\mathbf{x})$.

Trajectories in Region-II are those who pierce through the y axis directly with nonzero momentum $\mathbf{p}$ and their actions lie in the intervals denoted by number 2 in Fig. 3. Region-II is bounded by the MPEPs approaching $(0, 0)$ asymptotically. Subsequent investigations on MPEP show that their momentums $\mathbf{p}$ tend to zero in the vicinity of $(0, 0)$, implying their locations on the intersections of the unstable manifold of the initial state and the stable manifold of final state. Therefore MPEPs are heteroclitic trajectories. Actions in Region-III are of the same order as in Region-I, indicating that escape does not occur either. However, motions of trajectories in Region-III are remarkably distinguished from those of Region-I and even Region-IV. Let us discuss them in detail with a schematic illustration shown in Fig. 4. A trajectory in Region-III, plotted by

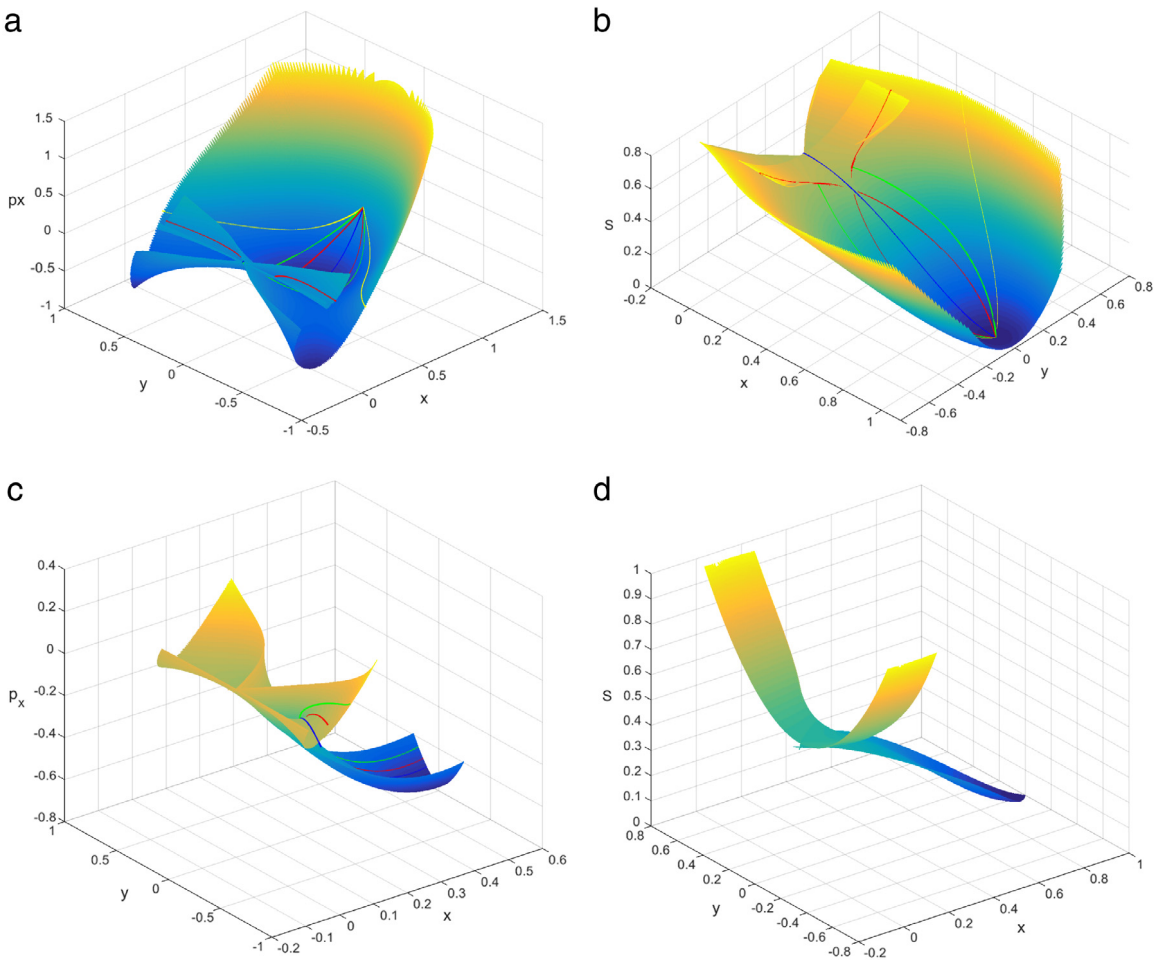

Fig. 5. (a) The Lagrangian manifold of the fluctuational paths. $\alpha = 10$ (b) The action surface. Typical trajectories in Fig. 2 dividing the pattern are also plotted. (c) Parts of the Lagrangian manifold where a folding structure arises. (d) Parts of the action surface where there exists multi-valuedness.

a blue line in Fig. 4, fluctuates toward the separatrix first and then turn back until it encounters the caustics. As a contrast, trajectories from Region-IV encounter caustics during their fluctuations toward the separatrix, see the yellow one in Fig. 4. Moreover, the latter ones proceed and escape from the basin of attraction while the former remain and move backwards. If we define a direction of the caustic by the directions of fluctuational paths to which the caustic is tangent, the caustics here go "away" from the cusp rather than toward it. This is the type-I cusp point due to Ref. [12] and the directions of caustics are shown in Fig. 4.

The Lagrangian manifold and action surface are shown in Fig. 5. We only plot the Lagrangian manifold in $x - y - p_x$ space in Fig. 5(a), with typical trajectories dividing the pattern also plotted in corresponding colors. The folding structures are clearly seen and to make it more evident, we plot this particular part in Fig. 5(c). It displays a structure of "bowknot" emerging from the cusp. The red line corresponds to the boundary trajectory separating Region-III and IV in Fig. 2. Two sample fluctuational trajectories are also plotted, with the green one from Region-III and the blue one from Region-IV. The action surface in Fig. 5(b) has a region of multi-valuedness, which is particularly shown in Fig. 5(d). The structure like a pair of "wings" just results from the trajectories of Region-III and IV.

5. Calculations of the quasi-potential

As discussed in Section 3, Eq. (8) specifies the form of the action functional defined in the space of all continuous functions mapping from $\left[t_0, t_f\right]$ to $\mathbf{R}^2$. For a general class of stochastic differential equations on $\mathbf{R}^n$ with drift vector b and diffusion tensor $a = \sigma\sigma^T$ as follows:

$$\mathrm{d}X^{\varepsilon}(t) = b\left(X^{\varepsilon}(t)\right)\mathrm{d}t + \sqrt{\varepsilon}\sigma\left(X^{\varepsilon}(t)\right)\mathrm{d}W(t) \tag{13}$$

the action functional is defined as

$$S_T(\psi) = \int_0^T L\left(\psi,\ \dot{\psi}\right)\ \mathrm{d}t \tag{14}$$

where the Lagrangian $L(x, y)$ is given by $L(x, y) = \left\langle y - b(x),\ a^{-1}(x)(y - b(x))\right\rangle/2$ and $\langle\cdot,\ \cdot\rangle$ denotes the Euclidean dot product in $\mathbf{R}^n$.

Due to the large deviation theory, the probability of the trajectory $X^\varepsilon(t),\ t \in [0, T],\ T < +\infty$ arriving in some Borel set B of $\mathbf{R}^n$ is estimated in the following way

$$P_x\{X^\varepsilon(t) \in B\} \sim \exp\left(-\varepsilon^{-1}\ \inf_{\psi}\ S_T(\psi)\right) \tag{15}$$

where $\sim$ denotes the logarithmic equivalence, i.e., $f(x) \sim \exp(\varepsilon g(x))$ if $\log f(x)/\varepsilon \to g(x)$ as $\varepsilon \to 0$. P_x is a conditional probability $P\{\cdot \mid X^\varepsilon(0) = x\}$. Actually this is just the essence of problems of noise induced fluctuations or escapes.

However, T in Eq. (15) is finite. We remark that the infimum is usually not attained under such circumstances since initial or end states can be equilibria or limit cycles, so that escapes could occur only on sufficient long time scales $\left[0,\ \exp\left(\varepsilon^{-1}C\right)\right]$ with some $C > 0$. Consequently, Freidlin and Wentzell introduced the quasi-potential which is defined as the minimization over both times and paths:

$$V(x_1, x_2) = \inf_{T>0}\ \inf_{\psi \in C_{x_1}^{x_2}(0,T)}\ S_T(\psi) \tag{16}$$

where $C_{x_1}^{x_2}(0, T)$ denotes the space of all absolutely continuous functions f on $[0, T]$ such that $f(0) = x_1,\ f(T) = x_2$.

An elaboration about the quasi-potential can be found in Ref. [8] and now let us just simply discuss its physical interpretations. As one can infer from its name, it plays a similar role as the potential for a gradient system, measuring the relative stability of separate metastable state. That is to say, the expected exit time for a gradient system from a domain of attraction of one of the metastable state exponentially depends on the depth of that potential well, i.e., the difference between the peak and the bottom of the potential [18]. As for non-gradient systems, we have similar results using quasi-potentials [8]:

$$\mathrm{E}[\tau_{exit}] \sim \exp\left(\varepsilon^{-1}\ \min_{x \in \partial U_{x_1}}\ V(x_1, x)\right) \tag{17}$$

where x_1 is an asymptotic stable point and ∂U_{x_1} denotes its basin boundary.

A realization of system (1) driven under noise of intensity $D = 0.3$ is shown in Fig. 6, with a histogram of the state variables during the whole simulating time [0, 6000] on the right side. It can be seen from the density that almost the same time is spent near $(-1, 0)$ as near $(1, 0)$, suggesting that the exit from one of them costs equal time from the other. This is in consistent with the symmetry of the deterministic vector field but still remains to be quantified. Next let us demonstrate it using the concept of quasi-potential.

Calculations of quasi-potential can be done by solving the static Hamilton–Jacobi equation, which is a formidable task. However, Cameron [19] proposed an algorithm to compute the quasi-potential on a regular mesh by adjusting the ordered upwind methods [20] which considers and accepts values of adjacent points in ascending orders. A pair of contour and 3D plots of the quasi-potential is given in Fig. 7. The values at both stable points $(\pm 1, 0)$ are zeros and the one at the origin is 0.4831, which agrees with the result given by the method of action plot in Section 4. See Fig. 3(b). We should remark that the quasi-potential by definition attains the infimum of the action functional, with other possible local minima disregarded.

6. Bifurcations of singularities

In this section we discuss the bifurcations of the singularities from a topological point of view, by investigating the variation of the structure of Lagrangian manifold. The positions of the cusp points on the x axis can also be determined.

Since the MPEP initially lie along the x axis, we expand the action $S(x, y)$ and the prefactor $C(x, y)$ in the WKB approximation (3) near the x axis in powers of y [14]:

$$\begin{aligned} S(x, y) &= f_0(x) + f_2(x)\, y^2/2 + O\left(y^4\right) \\ C(x, y) &= c_0(x) + c_2(x)\, y^2/2 + O\left(y^4\right) \end{aligned} \tag{18}$$

and the vector field $\mathbf{u}(x, y) = \left(x - x^3 - \alpha x y^2,\ -\mu y - x^2 y\right)$ is rewritten as:

$$\begin{aligned} u_x(x, y) &= v_0(x) + v_2(x)\, y^2 + O\left(y^4\right) \\ u_y(x, y) &= u_1(x)\, y + u_3(x)\, y^3 + O\left(y^5\right). \end{aligned} \tag{19}$$

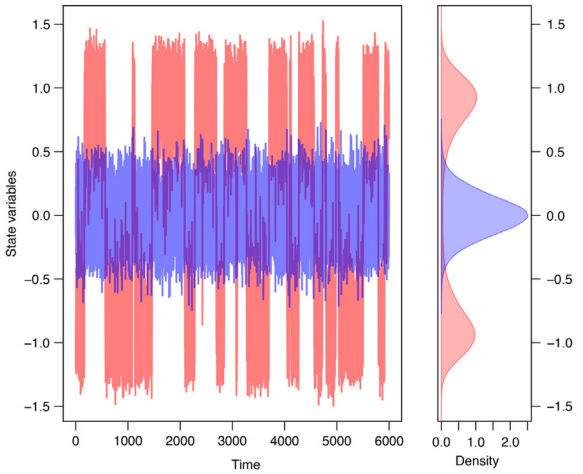

Fig. 6. A realization of system (1), with x in red and y in blue. The left side shows the time series and the right one shows a histogram of the x and y values over the entire realization. We set the noise intensity $D = 0.3$. (For interpretation of the references to color in this figure legend, the reader is referred to the web version of this article.)

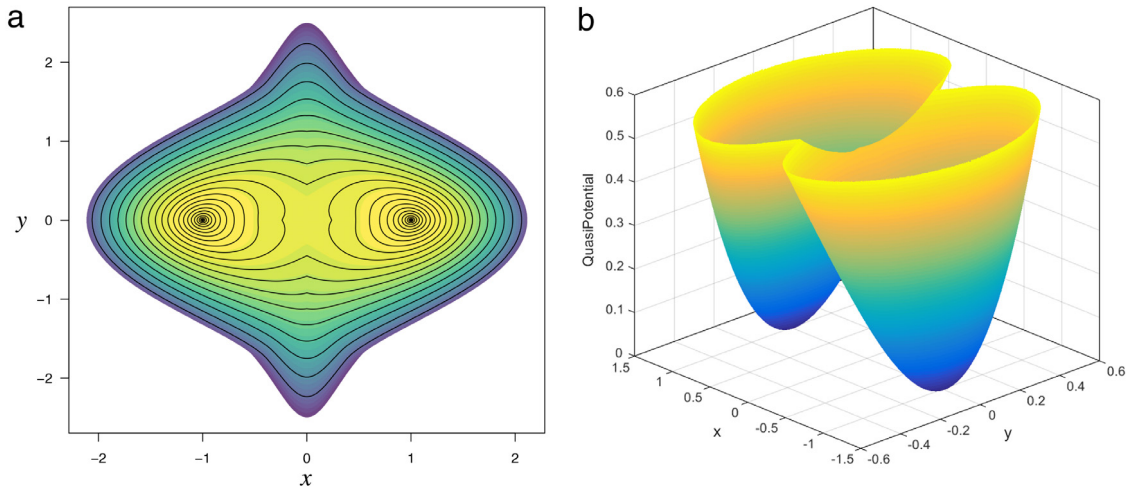

Fig. 7. (a) A contour plot of the quasi-potential of system (1). Yellow corresponds to low values and purple corresponds to high values. (b) A 3D plot to help visualize the quasi-potential. (For interpretation of the references to color in this figure legend, the reader is referred to the web version of this article.)

We remark that the forms of expansions above are due to the symmetry of the vector field and $f_2(x)$ measures the transverse length scale on which the probability density is non-negligible [14]. Clearly, $f_2(x) = \partial^2 S/\partial y^2(x, 0)$.

Substituting the WKB form of the expansion (18) into the Fokker–Planck equation one can obtain a transport equation for the prefactor $C(x, y)$, which is beyond the scope of this paper, and a nonlinear Riccati equation for $f_2(x)$:

$$\dot{f}_2 = -{f_2}^2 - 2u_1 f_2 + 4v_0 v_2 \tag{20}$$

where u_1, v_0, v_2 are define by (19). Eq. (20) describes the temporal evolution of the width where the WKB approximation is valid surrounding the MPEP, which now lies along the x axis by assumption. From the Hamiltonian system (12) it is straightforward to see that the MPEP along the x axis satisfies $\dot{x} = -v_0(x)$ ($p_x = -2v_0(x)$, $p_y = 0$). Therefore the time evolution of f_2 can be transformed into the position dependence in x.

To ensure the WKB approximation to be valid, $f_2(x)$ must remain positive along the entire MPEP. Considering the homogeneous form of Eq. (20) only, one obtains a stable state $\bar{f}_2 = -2u_1 > 0$ for all $x \in (0, 1]$ (the other is an unstable state $\bar{f}_2 = 0$). However, if the inhomogeneous term $4v_0 v_2$ is sufficiently negative in some portion of x axis, it can drive f_2 to zero before the saddle point $(0, 0)$ is reached [21]. Furthermore, f_2 will be driven to $-\infty$ under further integrations of (20). Recall that $2v_2 = \partial^2 u_x/\partial y^2(x, 0)$ (part of the inhomogeneous term), which is negative for $x \in (0, 1]$, increases the off-axis weakness and thus leads to the bifurcation of MPEP. If it is true, the positions where f_2 tends to $-\infty$ are exactly the positions of cusps, since the failure of the WKB expansion near the x axis is associated with the bifurcation of MPEP.

The plot of f_2 along the on-axis path is given in Fig. 8 for several parameters α. When $\alpha < 4$ it is evident that f_2 remains positive and finite from $x = 1$ to $x = 0$, converging to $\bar{f}_2(0) = -2u_1(0) = 2$ as the origin is approached. As $\alpha = 4$ f_2 is

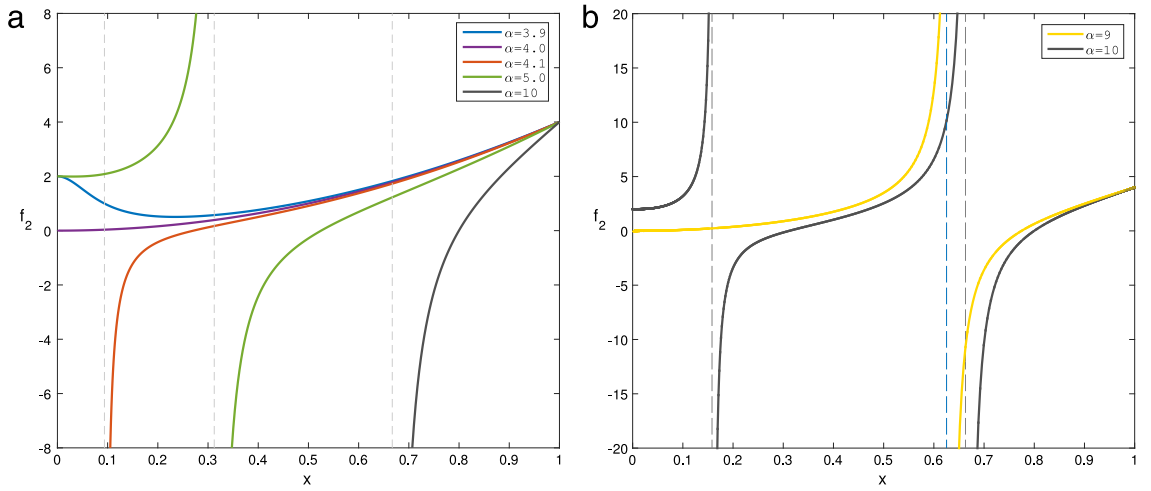

Fig. 8. (a) (b) The position dependence of $f_2\ (x)$ along the on-axis path $\dot{x} = -v_0\ (x)$ for several α from $x = 1$. The dashed lines are the asymptotic lines of f_2 tending to $-\infty$.

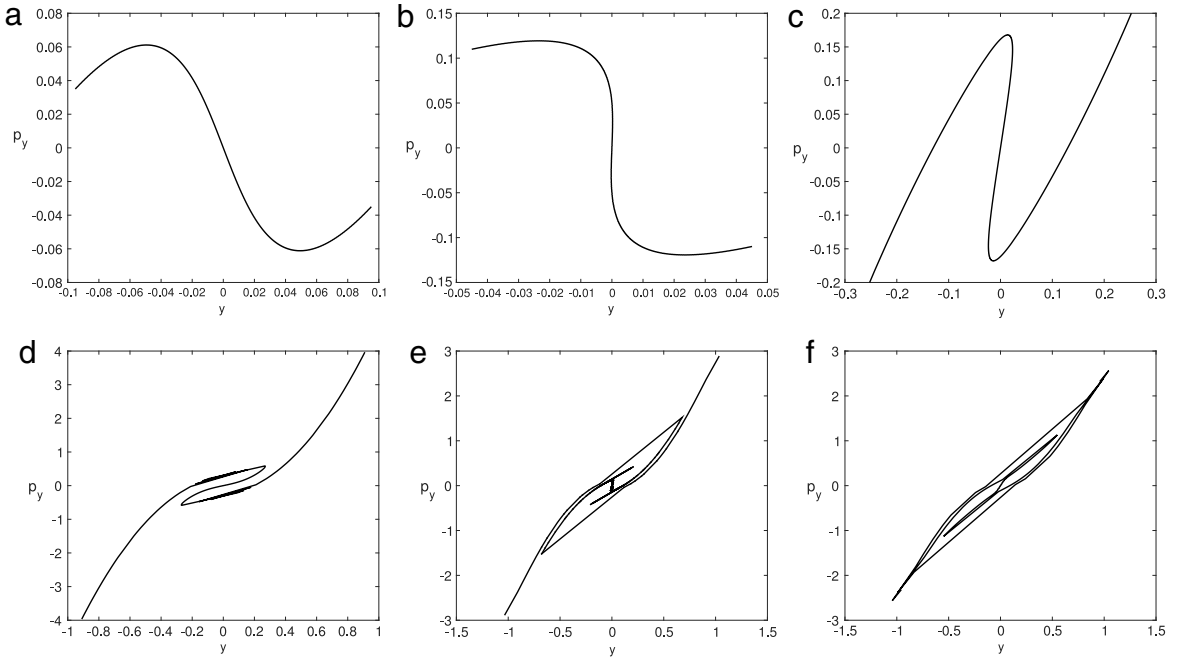

Fig. 9. Cross sections of the Lagrangian manifold along the x axis. (a) $\alpha = 5, x = 0.4$ (b) $\alpha = 5, x = 0.3124$ (c) $\alpha = 5, x = 0.25$ (d) $\alpha = 10, x = 0.4$ (e) $\alpha = 10, x = 0.158$ (f) $\alpha = 10, x = 0.115$.

driven to zero and for larger α, f_2 reaches zero at some positive x and then tends to $-\infty$. Our claim turns out to be true by a comparison between the position of the asymptotic line corresponding to $\alpha = 5$, given in Fig. 8(a), and the approximate position of cusp in Fig. 2. As α increases the cusp moves toward $x = 1$. Situations for $\alpha = 9$ are similar as $\alpha = 4$, with f_2 tending to zero at the origin, see Fig. 8(b). When $\alpha > 9$ a new cusp point appears from the origin and the previous cusp continues moving to $x = 1$.

Taking $f_2\ (x) = \partial^2 S/\partial y^2\ (x, 0) = \partial p_y/\partial y\ (x, 0)$ (see Eq. (4)) into account, we can regard f_2 as the slope of p_y. Consequently the evolution of f_2 along the x axis is equivalent to the clockwise rotation of p_y near $y = 0$ as x decreases. We have plotted the Lagrangian manifold in the space of $x - y - p_x$ in Fig. 5(a), and now we are in a position to consider the role of p_y. Several cross sections of the Lagrangian manifold in the $x - y - p_y$ with different values of x are shown in Fig. 9. Compare the slopes of the p_y at $y = 0$ with the values of f_2 in Fig. 8. The cross sections for Fig. 9(b) and (e) are selected near the corresponding cusps so that p_y are nearly vertical. In addition, every time when x passes a cusp point, the number of p_y for the same y near zero increases by two, from single value, to three values, to five values, etc. This implies that as we move toward the

separatrix along the x axis the Lagrangian manifold experiences a "twisting" process. As α increases the degree of twist is further intensified, creating a new cusp from the origin by each rotation.

7. Conclusion

In this paper we studied the noise-induced escape from a metastable state of a double-well model driven by white noise. Using the WKB approximation an axillary Hamiltonian system was obtained, trajectories of which are most probable fluctuational paths. The pattern of fluctuational paths was then plotted and divided into various regions by the method of action plot. Trajectories within different regions showed qualitatively distinguished behaviors, which were investigated in detail. The quasi-potential was computed via the ordered upwind method and the contour plot and 3D plot of the global one were shown. It illustrates the relative stabilities of the two metastable states and its value at the origin is equal to the one integrated along the MPEP. The Lagrangian manifold showed a "bowknot" structure with several asymptotic lines to y axis and the action surface displayed a property of multi-valuedness in some area corresponding to the region of the pattern where points were reachable via multiple fluctuational trajectories. The bifurcations of singularities as the parameter α varies were analytically studied by a nonlinear Riccati equation of f_2, the second-order term in the WKB expansion of $S(x, y)$. Its behaviors delineated the evolution of the Lagrangian manifold along the x axis, uncovering the successive twisting properties of the manifold. As α increases the twisting degree intensifies and new cusp point on the x axis is created over one rotation.

Acknowledgments

This research was supported by the National Natural Science Foundation of China (Grant No. 11472126, 11232007) and the Project Funded by the Priority Academic Program Development of Jiangsu Higher Education Institutions (PAPD).

References

[1] M.I. Dykman, P.V.E. McClintock, V.N. Smelyanski, N.D. Stein, N.G. Stocks, Optimal paths and the prehistory problem for large fluctuations in noise-driven systems, Phys. Rev. Lett. 68 (18) (1992) 2718.
[2] V. Chinarov, M. Dykman, V. Smelyanskiy, Dissipative corrections to escape probabilities of thermal-nonequilibrium systems, Phys. Rev. E 47 (4) (1993) 2448.
[3] S. Beri, R. Mannella, D.G. Luchinsky, A. Silchenko, P.V. McClintock, Solution of the boundary value problem for optimal escape in continuous stochastic systems and maps, Phys. Rev. E 72 (3) (2005) 036131.
[4] M. Dykman, V. Smelyanskiy, Distribution of fluctuational paths in noise-driven systems, Superlattices Microstruct. 23 (3/4) (1998) 495–504.
[5] S.J. Einchcomb, A.J. Mckane, Use of Hamiltonian mechanics in systems driven by colored noise, Phys. Rev. E 51 (4) (1995) 2974–2981.
[6] A.J. Mckane, H.C. Luckock, A.J. Bray, Path integrals and non-markov processes. i. general formalism, Phys. Rev. A 41 (2) (1990) 644–656.
[7] A.J. Bray, A.J. Mckane, T.J. Newman, Path integrals and non-markov processes. ii. escape rates and stationary distributions in the weak-noise limit, Phys. Rev. A 41 (2) (1990) 657–667.
[8] M.I. Freidlin, A.D. Wentzell, Random Perturbations of Dynamical Systems, Springer-Verlag, 2002.
[9] P. Grassberger, Noise-induced escape from attractors, J. Phys. A: Math. Gen. 22 (16) (1989) 3283–3290.
[10] M.I. Dykman, M.M. Millonas, V.N. Smelyanskiy, Observable and hidden singular features of large fluctuations in nonequilibrium systems, Phys. Lett. A 195 (1) (1994) 53–58.
[11] M.I. Dykman, D.G. Luchinsky, P.V. Mcclintock, V.N. Smelyanskiy, Corrals and critical behavior of the distribution of fluctuational paths, Phys. Rev. Lett. 77 (26) (1997) 5229–5232.
[12] V.N. Smelyanskiy, M.I. Dykman, R.S. Maier, Topological features of large fluctuations to the interior of a limit cycle, Phys. Rev. E 55 (3) (1997) 2369–2391.
[13] D.G. Luchinsky, R.S. Maier, R. Mannella, P.V.E. Mcclintock, D.L. Stein, Experiments on critical phenomena in a noisy exit problem, Phys. Rev. Lett. 79 (17) (1997) 3109–3112.
[14] R.S. Maier, D.L. Stein, Escape problem for irreversible systems, Phys. Rev. E 48 (2) (1993) 931–938.
[15] R.S. Maier, D.L. Stein, Effect of focusing and caustics on exit phenomena in systems lacking detailed balance, Phys. Rev. Lett. 71 (12) (1993) 1783–1786.
[16] R.S. Maier, D.L. Stein, A scaling theory of bifurcations in the symmetric weak-noise escape problem, J. Stat. Phys. 83 (3–4) (1996) 291–357.
[17] D.G. Luchinsky, R.S. Maier, R. Mannella, P.V.E. Mcclintock, D.L. Stein, Observation of saddle-point avoidance in noise-induced escape, Phys. Rev. Lett. 82 (9) (1999) 1806–1809.
[18] H.A. Kramers, Brownian motion in a field of force and the diffusion model of chemical reactions, Physica 7 (4) (1940) 284–304.
[19] M.K. Cameron, Finding the quasipotential for nongradient SDEs, Physica D 241 (18) (2012) 1532–1550.
[20] James A. Sethian, Alexander Vladimirsky, Ordered upwind methods for static Hamilton–Jacobi equations: Theory and algorithms, SIAM J. Numer. Anal. 41 (1) (2003) 325–363.
[21] R.S. Maier, D.L. Stein, Transition-rate theory for nongradient drift fields, Phys. Rev. Lett. 69 (26) (1992) 3691–3695.